Injury

Developmental Neuroscience

Dev Neurosci 2011;33:231–240
DOI: 10.1159/000328125

Received: September 13, 2010
Accepted after revision: March 25, 2011
Published online: July 28, 2011

Magnitude of [^{11}C]PK11195 Binding Is Related to Severity of Motor Deficits in a Rabbit Model of Cerebral Palsy Induced by Intrauterine Endotoxin Exposure

Sujatha Kannan[a, 1] Fadoua Saadani-Makki[a] Bindu Balakrishnan[a] Pulak Chakraborty[b] James Janisse[c] Xin Lu[a] Otto Muzik[a, b] Roberto Romero[d] Diane C. Chugani[a, b]

Departments of [a]Pediatrics, [b]Radiology and [c]Family Medicine and Public Health Sciences, Wayne State University, and [d]Perinatology Research Branch, Eunice Kennedy Shriver National Institute of Child Health and Human Development, NIH, United States Department of Health and Human Services, Detroit, Mich., USA

Key Words
Microglia · Positron emission tomography · Neuroinflammation · Cerebral palsy · Maternal inflammation

Abstract
Intrauterine inflammation is known to be a risk factor for the development of periventricular leukomalacia (PVL) and cerebral palsy. In recent years, activated microglial cells have been implicated in the pathogenesis of PVL and in the development of white matter injury. Clinical studies have shown the increased presence of activated microglial cells diffusely throughout the white matter in brains of patients with PVL. In vitro studies have reported that activated microglial cells induce oligodendrocyte damage and white matter injury by release of inflammatory cytokines, reactive nitrogen and oxygen species and the production of excitotoxic metabolites. PK11195 [1-(2-chlorophenyl)-*N*-methyl-*N*-(1-methylpropyl)-3-isoquinoline carboxamide] is a ligand that is selective for the 18-kDa translocator protein expressed on the outer mitochondrial membrane of activated microglia and macrophages. When labeled with carbon-11, [^{11}C]PK11195 can effectively be used as a ligand in positron emission tomography (PET) studies for the detection of activated microglial cells in various neuroinflammatory and neurodegenerative conditions. In this study, we hypothesized that the magnitude of [^{11}C]-*(R)*-PK11195 uptake in the newborn rabbit brain, as measured using a small-animal PET scanner, would match the severity of motor deficits resulting from intrauterine inflammation-induced perinatal brain injury. Pregnant New Zealand white rabbits were intrauterinely injected with endotoxin or saline at 28 days of gestation. Kits were born spontaneously at 31 days and underwent neurobehavioral testing and PET imaging following intravenous injection of the tracer [^{11}C]-*(R)*-PK11195 on the day of birth. The neurobehavioral scores were compared with the change in [^{11}C]PK11195 uptake over the time of scanning, for each of the kits. Upon analysis using receiver operating characteristic curves, an optimal combined sensitivity and specificity for detecting abnormal neurobehavioral scores suggestive of cerebral palsy in the neonatal rabbit was noted for a positive change in [^{11}C]PK11195 uptake in the brain over time on PET

[1] Corresponding author

Fax +41 61 306 12 34
E-Mail karger@karger.ch
www.karger.com

Accessible online at:
www.karger.com/dne

Assoc. Prof. Sujatha Kannan, MD
Department of Anesthesiology and Critical Care Medicine
Johns Hopkins Medical Institute
600N Wolfe Street, 904 Blalock, Baltimore, MD 21287 (USA)
E-Mail skannan.wsu@gmail.com

imaging (sensitivity of 100% and area under the curve of >0.82 for all parameters tested). The strongest agreements were noted between a positive uptake slope – indicating increased [^{11}C]PK11195 uptake over time – and worsening scores for measures of locomotion (indicated by hindlimb movement, forelimb movement, circular motion and straight-line motion; Cohen's $\kappa > 0.75$ for each) and feeding (indicated by ability to suck and swallow and turn the head during feeding; Cohen's $\kappa > 0.85$ for each). This was also associated with increased numbers of activated microglia (mean ratio ± SD of activated to total microglia: 0.96 ± 0.16 in the endotoxin group vs. 0.13 ± 0.08 in controls; $p < 0.001$) in the internal capsule and corona radiata. Our findings indicate that the magnitude of [^{11}C]PK11195 binding measured in vivo by PET imaging matches the severity of motor deficits in the neonatal rabbit. Molecular imaging of ongoing neuroinflammation in the neonatal period may be helpful as a screening biomarker for detecting patients at risk of developing cerebral palsy due to a perinatal insult.

Introduction

Inflammation is a characteristic feature of many degenerative disorders of the brain and is accompanied by the presence of activated microglial cells [1]. Maternal intrauterine infection or chorioamnionitis leads to a fetal systemic inflammatory response mediated by cytokines, which may result in the activation of microglial cells and injury to the developing brain [2–4]. Intrauterine inflammation has been recognized as one of the causes of perinatal brain injury leading to periventricular leukomalacia (PVL), resulting in lifelong disabilities such as cerebral palsy and cognitive impairment in the infant [5]. Recent evidence has shown that activated microglia may trigger white matter injury in the perinatal period [6–9].

Microglia, the resident macrophage cells of the brain, predominantly serve an immune surveillance function [10]. In the developing brain, amoeboid microglia are present in the white matter tracts from the late second trimester onward, decreasing in density in the postnatal period [11]. These microglial cells migrate to the cortex, where they are found in their 'quiescent' stage during adulthood. During development, activated microglia assume a supportive role in myelinogenesis and axonogenesis by stimulating the synthesis of myelin basic protein and the induction of laminin, an extracellular matrix molecule that enhances neurite outgrowth [12, 13]. However, the presence of activated microglia in the white matter tracts during development may also increase the vulnerability of the fetal brain to diverse brain insults. Microglial cells, when activated by proinflammatory cytokines, release oxidative and nitrosative products, and excitotoxic metabolites that can damage surrounding oligodendrocytes [14, 15]. Reactive microglia are associated with demyelinating and degenerative disorders such as multiple sclerosis and Alzheimer's disease [16, 17]. Increased expression of protein nitration and lipid peroxidation in premyelinating oligodendrocytes, accompanied by the presence of activated microglia, was noted in autopsy brain tissues of patients with PVL [18]. The close association of activated microglial cells with oligodendrocyte death in PVL necessitates the early detection of inflammatory processes in the fetal brain.

Activated microglia have upregulation of the 18-kDa translocator protein (TSPO; also known as peripheral benzodiazepine receptor) expression in their outer mitochondrial membrane [19–21]. Although the function of TSPO has not been defined clearly, it has been implicated in the regulation of cell death [22], mitochondrial respiration [23], cell growth and proliferation [24], steroidogenesis [25], and chemotaxis and cellular immunity [26, 27]. Isoquinoline ligands such as PK11195 [1-(2-chlorophenyl)-*N*-methyl-*N*-(1-methylpropyl)-3-isoquinoline carboxamide] bind TSPO [28] that are expressed on activated microglial cells. When labeled with carbon-11, PK11195 can be effectively used as a ligand in positron emission tomography (PET) studies, indicating the presence of activated microglia in acute inflammatory and neurodegenerative disorders [17, 21, 29–35]. Detection of activated microglial cells in vivo can provide valuable information regarding the extent of injury sustained in the perinatal period. The aim of this study was to evaluate the sensitivity, specificity and agreement between the measurement of [^{11}C]-*(R)*-PK11195 uptake in the brain and the severity of motor deficits determined by a behavioral rating paradigm previously described in our neonatal rabbit model of brain injury, induced by maternal intrauterine endotoxin administration.

Materials and Methods

Animal Model

All procedures were approved by the institutional animal care and use committee. New Zealand white rabbits with timed pregnancies (CoVance Research Products Inc., Kalamazoo, Mich., USA) underwent laparotomy on gestation day 28 (term pregnancy: 31–32 days) and were injected with 1 ml of saline solution (con-

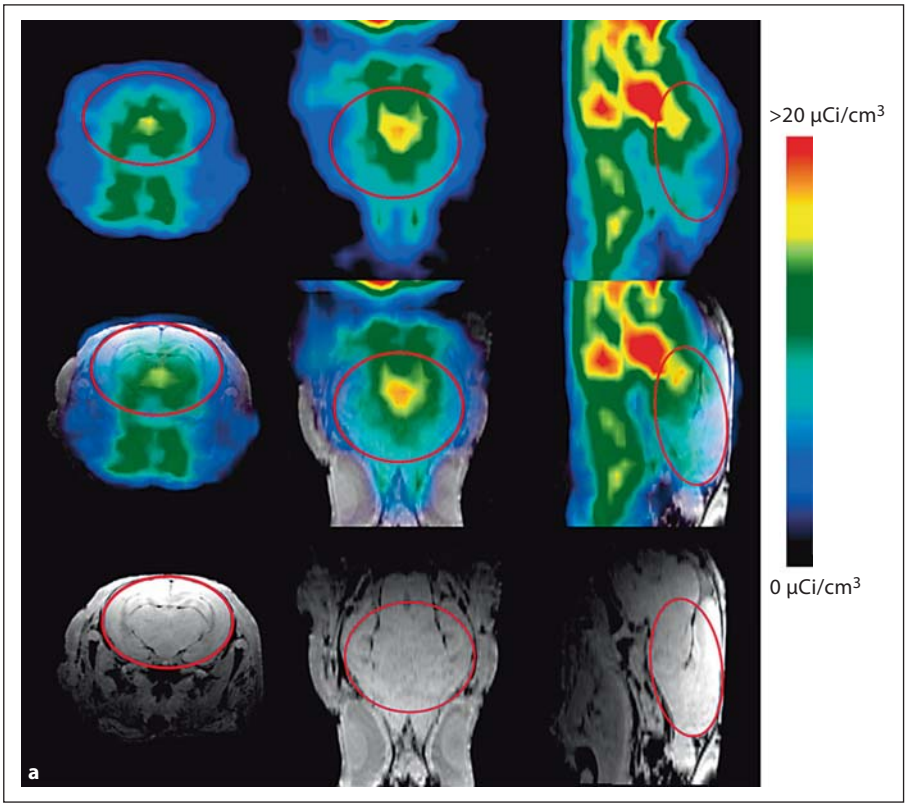

Fig. 1. a Coregistration of MR and PET images in representative newborn rabbit brain. PET (upper row) and MR images (lower row) along with the coregistered images (middle row) are shown for a representative endotoxin kit. The red solid circle indicates the region of interest (ROI) on the transverse planes (left column), and the red lines on the sagittal planes (right column) indicate the 3D ROI of the brain that was evaluated for [^{11}C]PK11195 uptake, which includes the cerebrum and midbrain. Middle column: Coronal planes.

trol saline group: n = 5) or 1 ml of saline containing 20 μg/kg of lipopolysaccharide (endotoxin group: n = 6; *Escherichia coli* serotype O127:B8; Sigma Aldrich, St. Louis, Mo., USA) along the length of the uterus between the fetuses, as previously described [8, 36]. A third group comprised animals that had no surgical intervention (control-no intervention: n = 3). All kits were born spontaneously on gestation day 31, and the litter size ranged from 8 to 12. One to 2 kits from each litter were randomly picked to undergo neurobehavioral testing and PET imaging with [^{11}C]PK11195 to determine the presence of neuroinflammation (the total number of kits imaged were 6 for control saline, 4 for control-no intervention, and 8 for endotoxin).

Neurobehavioral Scoring

Neurobehavioral testing and scoring was done, as previously described by Derrick et al. [37], before PET/MR imaging on the day of birth (n = 6 kits in the control saline group; n = 4 kits in the control-no intervention group; n = 8 kits in the endotoxin group). Briefly, the kits were videotaped for 5 min and scored on a scale of 0 (worst) to 3 (best) by 2 blinded observers for (1) posture (ability to maintain prone posture), (2) righting reflex (ability to right itself from supine to prone position for 10 attempts), (3) activity and locomotion on a flat surface (assessed by grading the quality, intensity and duration of spontaneous movement of the head as well as front and back legs), (4) ability to move in a straight line and in circles, (5) coordination of sucking and swallowing assessed by artificially feeding the rabbit kits with formula from a syringe with a dropper, and (6) ability to move the head during feeding. The tone on passive flexion and extension was assessed using the scoring based on the Ashworth scale, on which 0 indicated no increase in tone, and 4 indicated the limb was rigid in flexion or extension [37].

PET Imaging

PET scans were performed using a microPET R4 tomograph (Siemens Preclinical Solutions) followed by MRI for anatomic coregistration, as previously described [36]. In short, 3 fixed spheres attached to a head holder filled with fluid that was visible both on PET (radioactivity) and MR (water) images were used for coregistration of the two modalities. Following anesthesia with 0.1–0.2% isoflurane, the rabbit kits were positioned on the head holder and placed on the microPET bed as previously described [36]. The kits were injected intravenously with 10–20 MBq of [^{11}C]PK11195 (half-life: 20 min), and a 60-min list mode data acquisition in 3D mode was initiated. The list mode data were subsequently rebinned into discrete time frames (6 × 10 min), and attenuation-corrected sinograms reconstructed using the ordered subset expectation-maximization iterative algorithm, yielding an isotropic image resolution of about 2 mm full width at half maximum. Subsequently, each animal underwent MRI for coregistration with the PET images, as previously described [36].

The images were processed using the AMIDE software (A Medical Image Data Examiner, version 0.9.2). The MR and microPET image volumes were coregistered by manually matching the position of the 3 fiducial markers in both data sets (fig. 1a).

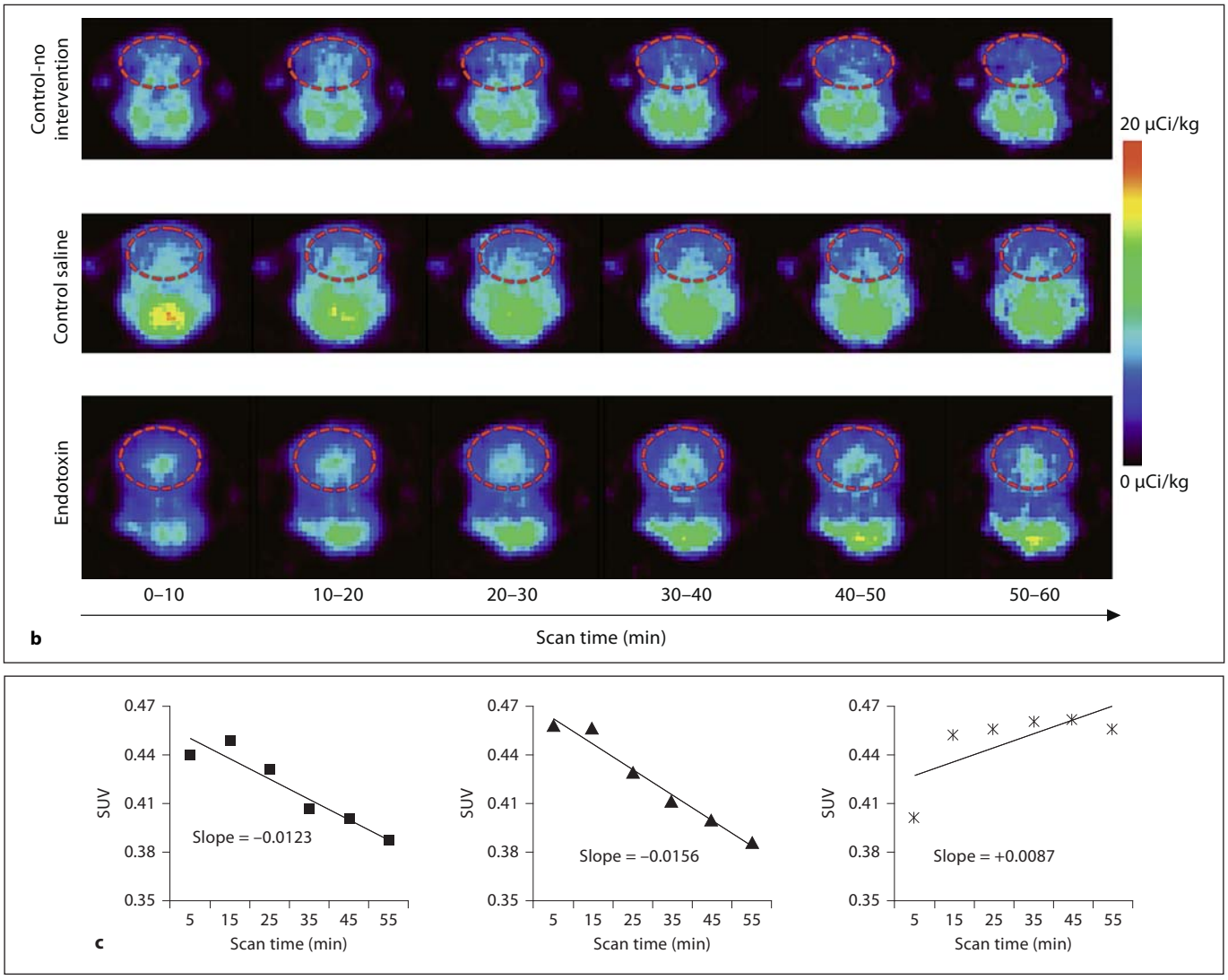

Fig. 1. b Representative PET images of [^{11}C]PK11195 uptake over time in newborn rabbit brain. A decrease in [^{11}C]PK11195 uptake in the brain is seen over the time of scanning (60 min) for control-no intervention (upper row) and control saline kits (middle row). In the endotoxin kits (lower row), an increase in tracer uptake is seen over time, indicating specific binding of the tracer to activated microglia in the brain of kits born to dams that were injected endotoxin in utero. The images are binned into 6 frames of 10 min each for analysis. The red dashed circle indicates the ROI involving the whole brain. **c** Representative slopes of [^{11}C]PK11195 uptake in the brain by PET imaging. The standard uptake value of [^{11}C]PK11195 activity in the brain of the kits in **b** is shown here. A decrease in [^{11}C]PK11195 uptake, resulting in a negative slope, is noted over the time period of scanning for both control groups, while an increase in uptake demonstrated by a positive slope is noted in the endotoxin kit (right), indicating specific binding of the tracer to activated microglia in the neonatal rabbit brain. Left: Control-no intervention group. Middle: Control saline group.

After coregistration, a 3D region of interest involving the whole brain (cerebrum and midbrain up to the brain stem) was defined in the MR image volumes and copied to the dynamic PET image sequences, yielding dynamic time-activity curves for the control and endotoxin groups. In order to avoid errors due to partial volume effects, only the region of the cerebrum and midbrain was included in the analysis, as previously described by our group [36]. The activity was standardized between animals by dividing the mean tracer concentration (in megabecquerels per cubic centimeter) at each time point by the injected activity (in megabecquerels) per weight (in grams) and expressed as standardized uptake values (SUV). The slope of the SUV curves derived from the whole acquisition period (0–60 min) was then used as a measure of microglial activation in the brain. Thus, a positive uptake slope

indicates specific binding of the tracer to the TSPO on activated microglia, while a negative uptake slope indicates initial accumulation of the tracer in tissue, followed by washout due to weak nonspecific binding.

Immunohistochemistry

Following PET imaging, the newborn rabbit kits were euthanized, perfused with 4% paraformaldehyde and cryoprotected. Microglial staining was done as previously described, using biotinylated *Lycopersicon esculentum* tomato lectin (1:100; Vector Laboratories, Burlingame, Calif., USA) followed by Vectastain ABC kit and color developed using 3,3-diaminobenzidine as peroxidase substrate (Vector Laboratories) [8, 36]. Microglial counting was done on 5 sections 180 μm apart, from the beginning of the lateral ventricle to the dorsal hippocampus (n = 5 kits from the endotoxin group; n = 5 kits from the control saline group). Six nonoverlapping fields across the corona radiata and internal capsule from both sides of the brain were captured using a Leica DM 2500 microscope equipped with a QImaging Retiga 2000R camera with a ×40 objective. Images were analyzed using Image-Pro Plus software, and microglia were counted in each region in a blinded manner. Data are expressed as the ratio of activated microglia (defined as cells with rounded or amoeboid morphology and retracted processes) to total microglia (ramified + rounded morphology) in each region. In addition, to demonstrate the presence of activated microglia, the microglial marker CD11b was assessed in endotoxin and control sections by staining with mouse monoclonal primary antibody (CD11b; 1:75; AbD Serotec, Raleigh, N.C., USA) and Alexa Fluor 488 goat anti-mouse (1:450; Invitrogen, Carlsbad, Calif., USA) as secondary antibody. Sections were stained with Alexa Fluor CD11b (green fluorescence), followed by tomato lectin tagged with Texas Red (red fluorescence; 1:100; Vector Laboratories), for detection of colocalization on microglia with 4′,6-diamidino-2-phenylindole (ProLong Gold antifade reagent with DAPI; Invitrogen) for nuclear staining.

Statistical Analyses

Prior to all analyses, the distribution of variables was examined, and all data were checked for accuracy and for outliers. For the receiver operating characteristic (ROC) analysis, all control and endotoxin kits were included (total: n = 18 kits). Initially, we assessed the relationship between the individual neurobehavioral scores and the uptake slope, using an ROC analysis. The neurobehavioral scores were assumed to represent the gold standard in the ROC analysis, with scores of 2 and above representing normal posture, locomotion, circular motion, straight-line movement, head movement, duration of activity, ability to suck and swallow and head turning during feeding. For hindlimb and forelimb tone, a score of 2 and below was assumed to represent normal tone, with values above 2 taken as hypertonia. Based on the ROC analysis, a cutoff point for the uptake slope was chosen (separating abnormal from normal uptake slope values), and Cohen's κ was calculated to assess the agreement between the dichotomized uptake slope values (normal, abnormal) and the dichotomized neurobehavioral scores. A κ value of 1.0 indicates perfect agreement between a particular measure and the gold standard, and positive values of κ indicate positive agreement between the measures. The strength of agreement (κ) is defined as: poor (<0.20), fair (0.21–0.40), moderate (0.41–0.60), substantial (0.61–0.80) and almost perfect (0.81–1.00) based on Landis and Koch [38]. The ratio of activated to total microglia was compared between the groups by using t tests. The data are reported as means ± SD for each of the groups.

Results

PET Imaging and Neurobehavioral Score

An increase in tracer activity over time was seen in the PET images and was expressed as a positive uptake slope of the SUV in the endotoxin kits (n = 8), while in the control kits (n = 10), a decrease in activity over time and a negative uptake slope were observed (fig. 1b, c). ROC analysis of the relationship between neurobehavioral scores and the uptake slope yielded a slope value of 0 as the best cutoff point, for which the accuracy was greatest. A positive uptake slope (indicating a steady increase in the amount of tracer bound to activated microglia) was associated with a worsening of neurobehavioral scores (fig. 2). Sensitivity and specificity pairs for the chosen cutoff value for the uptake slope (0) as well as the area under the curve for the various neurobehavioral parameters evaluated are shown in table 1. A substantial to almost perfect agreement between uptake slopes and neurological scores was seen for hindlimb and forelimb movement (κ = 0.71), straight-line motion (0.71), circular motion (0.98), ability to suck and swallow (0.82), and head turn during feeding (0.97). A moderate κ value was obtained for posture (κ = 0.47), forelimb and hindlimb tone (0.59), head movement (0.59) and duration of continuous activity in 1 min (0.47). The parameter that showed the lowest agreement was righting reflex (κ = 0.35). Although this was associated with a high sensitivity and area under the curve (table 1), it had the lowest specificity, indicating a higher rate of false positives.

Increased Activation of Microglial Cells in Endotoxin in the Corona Radiata and Internal Capsule

A robust increase in the number of microglia, along with a change in morphology, was observed in the internal capsule and corona radiata of endotoxin kits (fig. 3a, b). The activated microglial cells exhibited a change in morphology from ramified to amoeboid or round shape with retracted processes and enlarged somas, as previously described [8, 36]. The percent ratio of activated microglia (identified as amoeboid and rounded cells) to the total microglia counted (ramified + rounded) was significantly increased in the endotoxin kits when compared with the control saline kits (means ± SD of the ratio of activated

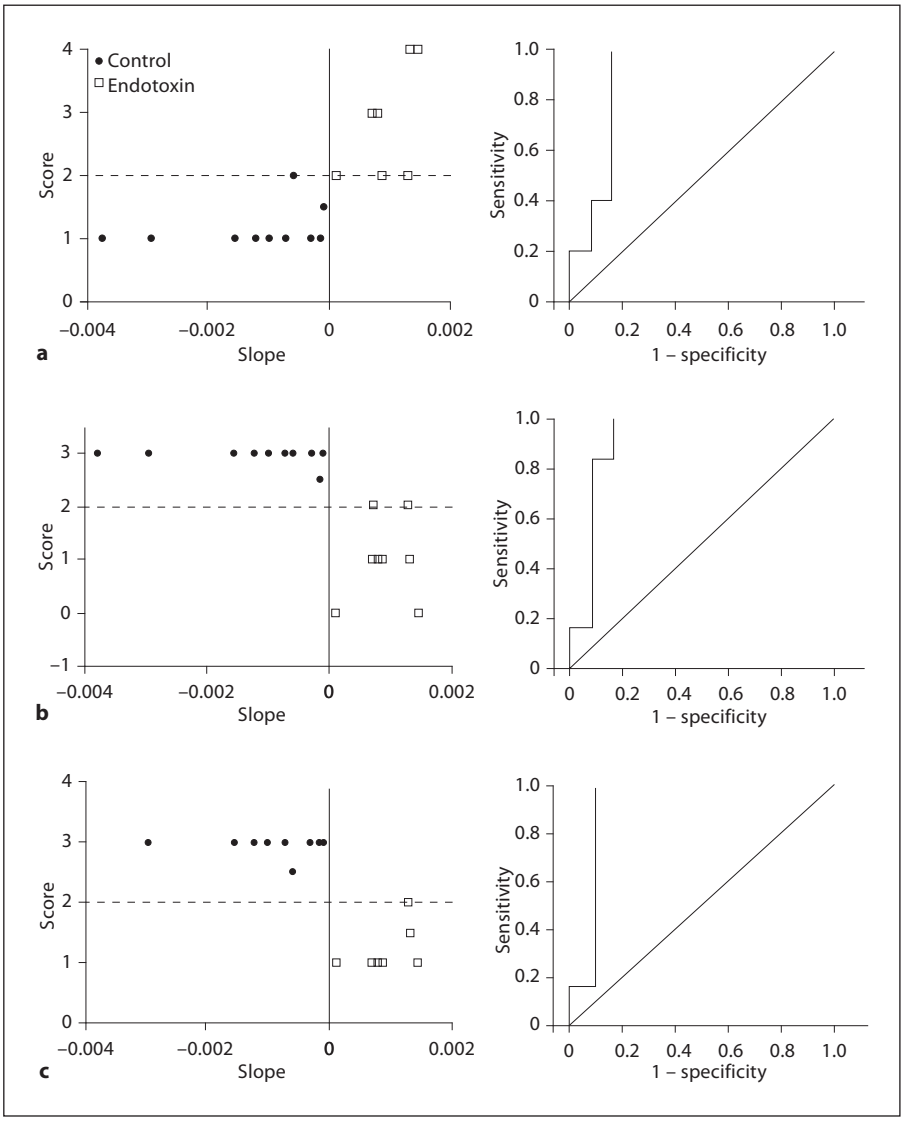

Fig. 2. Representative neurobehavioral graphs (left) along with the respective ROC curves (right). The neurobehavioral scores for each kit on day 1 were plotted against the uptake slope of [^{11}C]PK11195. Representative graphs (left) and ROC curves (right) for hindlimb tone (**a**), straight-line motion (**b**; as a measure of locomotion) and ability to suck and swallow (**c**; as a measure of feeding). Tone was evaluated from 0 (no increase in tone) to 4 (hypertonic, with limb rigid in flexion or extension), straight-line motion from 0 (worst, unable to move) to 3 (best, has full range of motion, maintains it for at least 3 steps) and ability to suck and swallow from 0 (worst, no jaw movement) to 4 (best, good coordination of sucking and swallowing) based on the scoring system described by Derrick et al. [37] for neonatal rabbit kits. Cutoff values for neurobehavioral scores were drawn at 2, as described in the text (≥2 was considered normal for straight-line motion and sucking and swallowing, and ≤2 was taken as normal for tone). For the PET-derived measure, a positive uptake slope (>0.00) was considered abnormal. There was substantial agreement between uptake slope and hindlimb tone (**a**, right; κ = 0.65), straight-line motion (**b**, right; κ = 0.77) and ability to suck and swallow (**c**, right; κ = 0.87).

Table 1. ROC values for each of the neurobehavioral parameters evaluated in newborn rabbit kits on day 1 of life

	Area under the curve	p	Sensitivity %	Specificity %	Agreement	p
Posture	0.91	0.015	100	71.4	0.53	0.011
Righting reflex	0.82	0.086	100	66.7	0.40	0.034
Forelimb tone	0.92	0.007	100	76.9	0.65	0.003
Hindlimb tone	0.89	0.012	100	76.9	0.65	0.003
Head movement	0.83	0.034	100	76.9	0.65	0.003
Hindlimb movement	0.92	0.005	100	83.3	0.77	0.001
Forelimb movement	0.92	0.005	100	83.3	0.77	0.001
Circular motion	1.00	<0.001	100	100	1.00	<0.001
Straight-line motion	0.92	0.005	100	83.3	0.77	0.001
Duration of activity for 1 min	0.86	0.034	100	71.4	0.53	0.011
Sucking and swallowing	0.92	0.007	100	90	0.87	<0.001
Head turn during feeding	1.00	0.001	100	100	1.00	<0.001

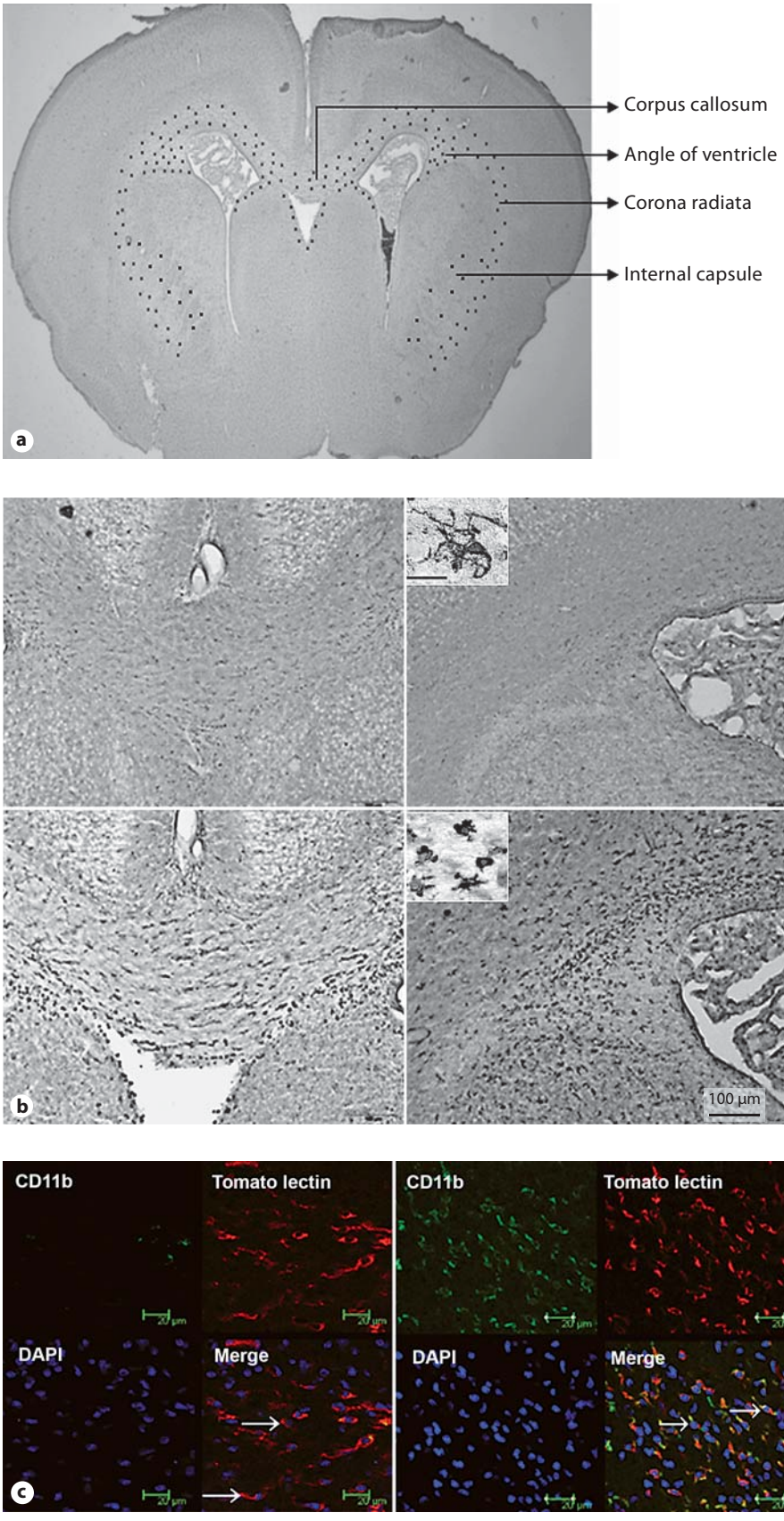

Fig. 3. a Schematic representation of the distribution of activated microglia in the newborn rabbit following intrauterine endotoxin administration. The image represents a coronal section of a newborn rabbit brain under low magnification. The distribution of activated microglia in the endotoxin-treated kits is indicated schematically by black dots in the corpus callosum, corona radiata and angle of the ventricle. At this level, microglia are found along the border of the ventricles, and in the corpus callosum, corona radiata and internal capsule. **b** Microglial staining in neonatal rabbits on day 1 of life. Slides were stained for microglia using *Lycopersicon esculentum* (tomato lectin). An intense increase in numbers of microglia and a change in morphology of the microglia to a more rounded and amoeboid form is noted in the corpus callosum, around the lateral ventricles and in the corona radiata in endotoxin kits when compared with controls. Left: Corpus callosum. Right: Angle of ventricle. Upper row: Control. Lower row: Endotoxin. Scale bar = 100 μm. **Insets** High-magnification image of the microglia, demonstrating the ramified morphology in controls (upper inset) and a more rounded and amoeboid/bushy morphology in the endotoxin kits (lower inset). Scale bar = 10 μm. **c** CD11b expression in the neonatal rabbit brain on day 1 of life. Representative sections from control (left) and endotoxin kits (right). Increased expression of CD11b in the periventricular region of endotoxin kits is shown when compared with the control saline kits on day 1 of life. Microglia labeled with tomato lectin (red fluorescence) colocalized with CD11b (green fluorescence) predominantly in the endotoxin kits and demonstrated a more rounded morphology (arrows, right), while microglial cells in the control kits were mostly ramified (arrows, left) and did not stain for CD11b. Scale bars = 20 μm.

to total microglia: 0.13 ± 0.08 in control saline kits vs. 0.96 ± 0.16 in endotoxin kits; $p < 0.001$). The presence of microglial activation in the endotoxin kits was confirmed by increased staining for the microglial β-integrin marker CD11b, which has been shown to be overexpressed by activated microglia in neuroinflammatory diseases [39, 40]. Most of the lectin-stained cells in the endotoxin kits had an amoeboid and rounded morphology and were strongly positive for CD11b staining. In contrast, the microglial cells in the control kits had a ramified morphology and demonstrated minimal staining for CD11b (fig. 3c).

Discussion

We have previously shown that intrauterine endotoxin administration near term results in motor deficits suggestive of cerebral palsy in neonatal rabbits [8]. We have also shown that microglial activation in the neonatal brain induced by maternal endotoxin administration can be detected in vivo by PET imaging [36]. In this study, we have demonstrated that increased uptake of [^{11}C]PK11195 indicated by a positive slope (>0.0) shows good agreement with decreased neurobehavioral scores and hypertonia in newborn kits. This was associated with an increase in the number of activated microglia in the corona radiata and internal capsule of the newborn brain upon immunohistochemistry, in kits exposed to maternal intrauterine endotoxin administration. Activated microglial cells may induce oligodendrocyte and neuronal injury by releasing oxidative and nitrosative products [18], by excitotoxic metabolites such as glutamate and quinolinic acid [14, 41, 42], and by producing a variety of proinflammatory cytokines, many of which are cytotoxic [43].

Microglia, the resident macrophage system of the brain, can ameliorate central nervous system repair or exacerbate an injury depending on the signals in the microenvironment. The dual role of microglia in the presence of brain injury has previously been shown [44]. The neurotoxic and proinflammatory effects of microglia through the production of reactive oxygen species via NADPH oxidase, cytokines (interleukin-1β, interleukin-6, tumor necrosis factor-α) and matrix metallopeptidase 9 may play a crucial role in neuronal and oligodendrocyte injury and in increasing blood-brain barrier permeability, thereby potentiating the injury. Microglia are known to produce various neurotrophic factors such as neurotrophins and growth factors (fibroblast growth factor, transforming growth factor-β_1), which are involved in neuronal survival and brain tissue repair in cases of brain injury [45–48]. The differential effects of microglia in response to an injury may be explained in terms of their phenotypic and functional heterogeneity. Thus, the predominant effect of a proinflammatory over an anti-inflammatory phenotype may be the impairment of the central nervous system repair mechanism by augmenting secondary damage [44, 49].

In this model, the increase in activated microglia is seen in association with maternal endotoxin administration. The high density of microglia normally present in the white matter tracts of rabbits at around 28 days' gestational age makes the surrounding oligodendrocytes vulnerable to the neurotoxic effects of activated microglia. Though it is still not clear whether the presence of activated microglia is the cause or the effect, its detection can be used as a reliable biomarker for brain injury in the perinatal period. In vivo detection of TSPO overexpression, which is constitutively expressed in very low levels in the normal healthy brain, has been used as a sensitive marker to visualize and measure microglial cell activation associated with various neuroinflammatory disorders [19–21]. In the presence of brain injury, the activation of microglial cells is typically localized to the site of the injured neuron, with extension along the anterograde or retrograde axonal pathway. This characteristic response helps to accurately localize the site and distribution of injury when imaging activated microglia, providing information about the temporal and spatial progression of various neuroinflammatory disorders. TSPO expression appears to be a more sensitive indicator of brain injury since an increase can be detected even before histological changes such as neuronal apoptosis or loss are noted [50].

Our study shows a strong agreement between the extent of [^{11}C]PK11195 uptake in the brain and the degree of motor impairment, indicating that this can be a sensitive biomarker for the presence of brain injury resulting in motor deficits. This is similar to previous studies that have shown that the extent of TSPO expression in the brain appears to be directly related to the extent of injury on histology, with a large increase noted in the case of frank neuronal loss and smaller increases noted with just the loss of neuronal terminals [50, 51]. One of the limitations of this study is that the PET imaging and neurobehavioral analysis was done at the same time. Ongoing studies evaluating the neurobehavioral function of the rabbits at adulthood would be helpful in further determining whether this imaging technique can be used as a predictor for determining long-term neurological outcome.

Detection of activated microglial cells in vivo can potentially provide valuable information about the degree

of injury sustained in the perinatal period. Neonates born to mothers with chorioamnionitis, either diagnosed clinically or by placental histopathology, can be screened by PET imaging with [^{11}C]-*(R)*-PK11195 for the presence of activated microglial cells as an indicator of neuroinflammation and possible predictor of the development of brain injury secondary to intrauterine infection. Though high radiation exposure in the neonatal period is a matter of concern with regard to the radiation dose, [^{11}C]-*(R)*-PK11195 scans in neonates could be accomplished using effective doses that are not much higher than the average annual background radiation exposure, which is around 3.6 mSv per person in the USA [52, 53]. The typical effective dose used in a PET scan is 5 mSv, which is less than in a clinical CT scan. A single clinical CT scan of the head typically results in a radiation exposure to about 30 mSv of the brain in a neonate, with doses as high as 90 mSv, depending on the number of scans/studies required [54]. With these dose exposures (30–90 mSv) in the newborn period, the lifetime attributable risk of radiation-associated cancer is around 0.04–0.06% [54]. This risk decreases substantially with a decrease in the dose used. Given the very serious, debilitating consequences of the development of cerebral palsy from perinatal brain injury, PET scanning for early detection of neuroinflammation in the neonate may potentially have a high benefit-to-risk ratio.

In conclusion, detection of activated microglia by PET imaging is a sensitive biomarker for indicating brain injury in the perinatal period. PET imaging for detection of neuroinflammation can be a valuable tool not only for noninvasively diagnosing the presence and extent of brain injury in newborns exposed to intrauterine insults, but also for directing appropriate, relevant supportive therapies. In conjunction with diffusion tensor imaging or MR spectroscopy, it can be used to detect subtle changes in the central nervous system that may not be obvious by conventional imaging techniques. Future studies in newborns exposed to chorioamnionitis, or at risk of neuroinflammation, would help in demonstrating whether [^{11}C]PK11195 uptake can be used as a biomarker for predicting long-term neurological outcome.

Acknowledgments

This study was funded in part by the National Institute of Child Health and Human Development, NIH (1K08HD050652), and the Perinatology Research Branch, Eunice Kennedy Shriver National Institute of Child Health and Human Development, NIH, United States Department of Health and Human Services. We would like to thank Dr. Amar Jyoti for his help with the immunohistochemistry.

References

1 Ladeby R, Wirenfeldt M, Garcia-Ovejero D, Fenger C, Dissing-Olesen L, Dalmau I, Finsen B: Microglial cell population dynamics in the injured adult central nervous system. Brain Res Brain Res Rev 2005;48:196–206.
2 Leviton A, Gilles F: Maternal urinary-tract infections and fetal leukoencephalopathy. N Engl J Med 1979;301:661.
3 Yoon BH, Romero R, Park JS, Kim CJ, Kim SH, Choi JH, Han TR: Fetal exposure to an intra-amniotic inflammation and the development of cerebral palsy at the age of three years. Am J Obstet Gynecol 2000;182:675–681.
4 Malaeb S, Dammann O: Fetal inflammatory response and brain injury in the preterm newborn. J Child Neurol 2009;24:1119–1126.
5 Wu YW, Escobar GJ, Grether JK, Croen LA, Greene JD, Newman TB: Chorioamnionitis and cerebral palsy in term and near-term infants. JAMA 2003;290:2677–2684.
6 Bell MJ, Hallenbeck JM: Effects of intrauterine inflammation on developing rat brain. J Neurosci Res 2002;70:570–579.
7 Cai Z, Pan ZL, Pang Y, Evans OB, Rhodes PG: Cytokine induction in fetal rat brains and brain injury in neonatal rats after maternal lipopolysaccharide administration. Pediatr Res 2000;47:64–72.
8 Saadani-Makki F, Kannan S, Lu X, Janisse J, Dawe E, Edwin S, Romero R, Chugani D: Intrauterine administration of endotoxin leads to motor deficits in a rabbit model: a link between prenatal infection and cerebral palsy. Am J Obstet Gynecol 2008;199:651e1–651e7.
9 Hagberg H, Peebles D, Mallard C: Models of white matter injury: comparison of infectious, hypoxic-ischemic, and excitotoxic insults. Ment Retard Dev Disabil Res Rev 2002; 8:30–38.
10 Aloisi F: The role of microglia and astrocytes in CNS immune surveillance and immunopathology. Adv Exp Med Biol 1999;468:123–133.
11 Billiards SS, Haynes RL, Folkerth RD, Trachtenberg FL, Liu LG, Volpe JJ, Kinney HC: Development of microglia in the cerebral white matter of the human fetus and infant. J Comp Neurol 2006;497:199–208.
12 Hamilton SP, Rome LH: Stimulation of in vitro myelin synthesis by microglia. Glia 1994; 11:326–335.
13 Masuda-Nakagawa LM, Muller KJ, Nicholls JG: Axonal sprouting and laminin appearance after destruction of glial sheaths. Proc Natl Acad Sci USA 1993;90:4966–4970.
14 Espey MG, Chernyshev ON, Reinhard JF Jr, Namboodiri MA, Colton CA: Activated human microglia produce the excitotoxin quinolinic acid. Neuroreport 1997;8:431–434.
15 Li J, Baud O, Vartanian T, Volpe JJ, Rosenberg PA: Peroxynitrite generated by inducible nitric oxide synthase and NADPH oxidase mediates microglial toxicity to oligodendrocytes. Proc Natl Acad Sci USA 2005; 102:9936–9941.
16 Hovelmeyer N, Hao Z, Kranidioti K, Kassiotis G, Buch T, Frommer F, von Hoch L, Kramer D, Minichiello L, Kollias G, Lassmann H, Waisman A: Apoptosis of oligodendrocytes via Fas and TNF-R1 is a key event in the induction of experimental autoimmune encephalomyelitis. J Immunol 2005; 175:5875–5884.

17 Stoll G, Jander S: The role of microglia and macrophages in the pathophysiology of the CNS. Prog Neurobiol 1999;58:233–247.
18 Haynes RL, Folkerth RD, Keefe RJ, Sung I, Swzeda LI, Rosenberg PA, Volpe JJ, Kinney HC: Nitrosative and oxidative injury to premyelinating oligodendrocytes in periventricular leukomalacia. J Neuropathol Exp Neurol 2003;62:441–450.
19 Banati RB, Goerres GW, Myers R, Gunn RN, Turkheimer FE, Kreutzberg GW, Brooks DJ, Jones T, Duncan JS: [^{11}C]*(R)*-PK11195 positron emission tomography imaging of activated microglia in vivo in Rasmussen's encephalitis. Neurology 1999;53:2199–2203.
20 Banati RB: Visualising microglial activation in vivo. Glia 2002;40:206–217.
21 Gerhard A, Banati RB, Goerres GB, Cagnin A, Myers R, Gunn RN, Turkheimer F, Good CD, Mathias CJ, Quinn N, Schwarz J, Brooks DJ: [^{11}C]*(R)*-PK11195 PET imaging of microglial activation in multiple system atrophy. Neurology 2003;61:686–689.
22 McEnery MW, Snowman AM, Trifiletti RR, Snyder SH: Isolation of the mitochondrial benzodiazepine receptor: association with the voltage-dependent anion channel and the adenine nucleotide carrier. Proc Natl Acad Sci USA 1992;89:3170–3174.
23 Hirsch JD, Beyer CF, Malkowitz L, Beer B, Blume AJ: Mitochondrial benzodiazepine receptors mediate inhibition of mitochondrial respiratory control. Mol Pharmacol 1989;35:157–163.
24 Wang JK, Morgan JI, Spector S: Benzodiazepines that bind at peripheral sites inhibit cell proliferation. Proc Natl Acad Sci USA 1984;81:753–756.
25 Papadopoulos V, Widmaier EP, Amri H, Zilz A, Li H, Culty M, Castello R, Philip GH, Sridaran R, Drieu K: In vivo studies on the role of the peripheral benzodiazepine receptor (PBR) in steroidogenesis. Endocr Res 1998; 24:479–487.
26 Lenfant M, Haumont J, Zavala F: In vivo immunomodulating activity of PK 1195, a structurally unrelated ligand for 'peripheral' benzodiazepine binding sites. 1. Potentiation in mice of the humoral response to sheep red blood cells. Int J Immunopharmacol 1986;8:825–828.
27 Ruff MR, Pert CB, Weber RJ, Wahl LM, Wahl SM, Paul SM: Benzodiazepine receptor-mediated chemotaxis of human monocytes. Science 1985;229:1281–1283.
28 Venneti S, Lopresti BJ, Wiley CA: The peripheral benzodiazepine receptor (Translocator protein 18kDa) in microglia: from pathology to imaging. Prog Neurobiol 2006;80: 308–322.
29 Banati RB, Newcombe J, Gunn RN, Cagnin A, Turkheimer F, Heppner F, Price G, Wegner F, Giovannoni G, Miller DH, Perkin GD, Smith T, Hewson AK, Bydder G, Kreutzberg GW, Jones T, Cuzner ML, Myers R: The peripheral benzodiazepine binding site in the brain in multiple sclerosis: quantitative in vivo imaging of microglia as a measure of disease activity. Brain 2000;123(pt 11):2321–2337.
30 Chen MK, Guilarte TR: Imaging the peripheral benzodiazepine receptor response in central nervous system demyelination and remyelination. Toxicol Sci 2006;91: 532–539.
31 Gerhard A, Pavese N, Hotton G, Turkheimer F, Es M, Hammers A, Eggert K, Oertel W, Banati RB, Brooks DJ: In vivo imaging of microglial activation with [^{11}C]*(R)*-PK11195 PET in idiopathic Parkinson's disease. Neurobiol Dis 2006;21:404–412.
32 Cagnin A, Myers R, Gunn RN, Lawrence AD, Stevens T, Kreutzberg GW, Jones T, Banati RB: In vivo visualization of activated glia by [^{11}C] *(R)*-PK11195-PET following herpes encephalitis reveals projected neuronal damage beyond the primary focal lesion. Brain 2001;124:2014–2027.
33 Edison P, Archer HA, Gerhard A, Hinz R, Pavese N, Turkheimer FE, Hammers A, Tai YF, Fox N, Kennedy A, Rossor M, Brooks DJ: Microglia, amyloid, and cognition in Alzheimer's disease: an [^{11}C]*(R)*PK11195-PET and [^{11}C]PIB-PET study. Neurobiol Dis 2008; 32:412–419.
34 Okello A, Edison P, Archer HA, Turkheimer FE, Kennedy J, Bullock R, Walker Z, Kennedy A, Fox N, Rossor M, Brooks DJ: Microglial activation and amyloid deposition in mild cognitive impairment: a PET study. Neurology 2009;72:56–62.
35 van Berckel BN, Bossong MG, Boellaard R, Kloet R, Schuitemaker A, Caspers E, Luurtsema G, Windhorst AD, Cahn W, Lammertsma AA, Kahn RS: Microglia activation in recent-onset schizophrenia: a quantitative *(R)*-[^{11}C]PK11195 positron emission tomography study. Biol Psychiatry 2008;64:820–822.
36 Kannan S, Saadani-Makki F, Muzik O, Chakraborty P, Mangner TJ, Janisse J, Romero R, Chugani DC: Microglial activation in perinatal rabbit brain induced by intrauterine inflammation: detection with ^{11}C-*(R)*-PK11195 and small-animal PET. J Nucl Med 2007;48:946–954.
37 Derrick M, Luo NL, Bregman JC, Jilling T, Ji X, Fisher K, Gladson CL, Beardsley DJ, Murdoch G, Back SA, Tan S: Preterm fetal hypoxia-ischemia causes hypertonia and motor deficits in the neonatal rabbit: a model for human cerebral palsy? J Neurosci 2004;24: 24–34.
38 Landis JR, Koch GG: The measurement of observer agreement for categorical data. Biometrics 1977;33:159–174.
39 Roy A, Fung YK, Liu X, Pahan K: Up-regulation of microglial CD11b expression by nitric oxide. J Biol Chem 2006;281:14971–14980.
40 Zhang SC, Goetz BD, Carre JL, Duncan ID: Reactive microglia in dysmyelination and demyelination. Glia 2001;34:101–109.
41 Barger SW, Goodwin ME, Porter MM, Beggs ML: Glutamate release from activated microglia requires the oxidative burst and lipid peroxidation. J Neurochem 2007;101:1205–1213.
42 Káradóttir R, Cavelier P, Bergersen LH, Attwell D: NMDA receptors are expressed in oligodendrocytes and activated in ischaemia. Nature 2005;438:1162–1166.
43 Imamura K, Hishikawa N, Ono K, Suzuki H, Sawada M, Nagatsu T, Yoshida M, Hashizume Y: Cytokine production of activated microglia and decrease in neurotrophic factors of neurons in the hippocampus of Lewy body disease brains. Acta Neuropathol 2005; 109:141–150.
44 Kigerl KA, Gensel JC, Ankeny DP, Alexander JK, Donnelly DJ, Popovich PG: Identification of two distinct macrophage subsets with divergent effects causing either neurotoxicity or regeneration in the injured mouse spinal cord. J Neurosci 2009;29:13435–13444.
45 Dean JM, Wang X, Kaindl AM, Gressens P, Fleiss B, Hagberg H, Mallard C: Microglial *MyD88* signaling regulates acute neuronal toxicity of LPS-stimulated microglia in vitro. Brain Behav Immun 2010;24:776–783.
46 Liang J, Takeuchi H, Jin S, Noda M, Li H, Doi Y, Kawanokuchi J, Sonobe Y, Mizuno T, Suzumura A: Glutamate induces neurotrophic factor production from microglia via protein kinase C pathway. Brain Res 2010;1322:8–23.
47 Sawada M, Kondo N, Suzumura A, Marunouchi T: Production of tumor necrosis factor-α by microglia and astrocytes in culture. Brain Res 1989;491:394–397.
48 Shimojo M, Nakajima K, Takei N, Hamanoue M, Kohsaka S: Production of basic fibroblast growth factor in cultured rat brain microglia. Neurosci Lett 1991;123:229–231.
49 Michelucci A, Heurtaux T, Grandbarbe L, Morga E, Heuschling P: Characterization of the microglial phenotype under specific pro-inflammatory and anti-inflammatory conditions: effects of oligomeric and fibrillar amyloid-β. J Neuroimmunol 2009;210:3–12.
50 Chen MK, Baidoo K, Verina T, Guilarte TR: Peripheral benzodiazepine receptor imaging in CNS demyelination: functional implications of anatomical and cellular localization. Brain 2004;127:1379–1392.
51 Kuhlmann AC, Guilarte TR: Cellular and subcellular localization of peripheral benzodiazepine receptors after trimethyltin neurotoxicity. J Neurochem 2000;74:1694–1704.
52 Ionizing radiation exposure of the population of the United States. NCRP Report No 93. National Council on Radiation Protection and Measurements, 1987.
53 Radiation: risks and realities. Document No EPA-402-K-07-006. US Environmental Protection Agency, 2007.
54 Brenner DJ, Hall EJ: Computed tomography: an increasing source of radiation exposure. N Engl J Med 2007;357:2277–2284.